Geophysical Research Letters

RESEARCH LETTER
10.1029/2022GL100574

Key Points:

- A common method for isolating the internal component of Atlantic Multidecadal Variability is to remove fluctuations associated with global-mean temperature
- This method introduces spurious Indo-Pacific connections in model Large Ensembles and observations due to internal variations in global-mean temperature
- A revised method based on removing fluctuations associated with the forced component of global-mean temperature mitigates this issue

Supporting Information:

Supporting Information may be found in the online version of this article.

Correspondence to:

C. Deser,
cdeser@ucar.edu

Citation:

Deser, C., & Phillips, A. S. (2023). Spurious Indo-Pacific connections to internal Atlantic Multidecadal Variability introduced by the global temperature residual method. *Geophysical Research Letters*, *50*, e2022GL100574. https://doi.org/10.1029/2022GL100574

Received 24 JUL 2022
Accepted 14 JAN 2023

Author Contributions:

Conceptualization: Clara Deser
Data curation: Adam S. Phillips
Formal analysis: Clara Deser
Investigation: Clara Deser
Methodology: Clara Deser
Software: Adam S. Phillips
Visualization: Adam S. Phillips
Writing – original draft: Clara Deser

Spurious Indo-Pacific Connections to Internal Atlantic Multidecadal Variability Introduced by the Global Temperature Residual Method

Clara Deser[1] **and Adam S. Phillips**[1]

[1]National Center for Atmospheric Research, Boulder, CO, USA

Abstract The relative contributions of external forcing and internal processes to the observed spatial and temporal characteristics of "Atlantic Multidecadal Variability" (AMV) are still under debate. Here, the efficacy of the commonly-used "global temperature residual method" for isolating the internal component of AMV is investigated by means of model Large Ensembles where the truth is known a priori. In this method, local sea surface temperature variability associated with global-mean temperature (*G*) is removed via linear regression, and the residuals regressed upon the North Atlantic residual timeseries. We show that this method introduces spurious connections over the Indo-Pacific due to the fact that *G* in any single realization includes both external and internal components: the latter dominated by influences from Pacific Decadal Variability independent of AMV. This methodological shortcoming can be overcome by using the forced component of *G* in the residual method applied to individual model realizations and to observations.

Plain Language Summary The phenomenon known as "Atlantic Multidecadal Variability" (AMV) has been widely studied and has important climate effects over Africa, Asia, Europe, and eastern North America. Recently, there has been considerable debate regarding the relative contributions of natural processes within the coupled ocean-atmosphere system versus human influences related to aerosol emissions on the spatial and temporal character of AMV. An accurate separation of these natural and anthropogenic contributions has proven challenging due to limitations of the data record. Statistical techniques aimed at isolating the natural component of AMV often yield conflicting results. Here, we investigate one widely-used approach based on removing variability associated with global-mean temperatures. We show that the conventional application of this method aliases another well-known phenomenon, "Interdecadal Pacific Variability," onto the pattern of natural AMV. However, with a simple modification to the method, the true pattern of natural AMV can be recovered.

1. Introduction

The climate phenomenon known as "Atlantic Multidecadal Variability" (AMV) is characterized by basin-scale fluctuations in sea surface temperatures (SSTs) over the North Atlantic, accompanied by changes in atmospheric circulation and associated hydrological impacts over Africa, Europe, and eastern North America [for example, Zhang et al., 2019 (Z19) and references therein]. The spatial and temporal characteristics of AMV derive from processes internal to the coupled ocean-atmosphere coupled system, and are also influenced by external radiative forcing, primarily anthropogenic aerosols [for example, Qin et al., 2020 (Q20) and references therein]. However, quantifying the relative contributions of internal and external drivers of AMV remains an ongoing challenge, with implications for prediction. Statistical approaches aimed at separating forced and internal components of observed AMV are sensitive to methodological choices, leading to conflicting results (e.g., Frankignoul et al., 2017). In particular, simple procedures such as subtracting global-mean temperature (Trenberth & Shea, 2006) or linear detrending (Enfield et al., 2001; Murphy et al., 2017) alias the pattern of forced climate change onto the structure of internal AMV (iAMV) as shown by Deser and Phillips (2021; hereafter DP21) and Baek et al. (2022). The modeling framework of "Single Model Initial-condition Large Ensembles" (LEs; Deser et al., 2020), which provides a priori knowledge of forced and internal contributions in any individual simulation, has served as an effective testbed for evaluating these and other methods (Baek et al., 2022; DP21; Frankignoul et al., 2017; Q20).

Another simple and widely-used empirical technique for isolating iAMV (and internal variability in general) is the "global temperature residual method" (G-Res method), which employs linear regression analysis to remove variability at each location that is linearly congruent with variability in global-mean SST (G; DP21; Q20; Yan

et al., 2019; Z19). The resulting "residual" SST anomalies are then used to construct an iAMV index timeseries [typically, the North Atlantic (NA; 0°–60°N, 80°W–0°E) area-average], and an associated iAMV spatial pattern obtained by regressing the residual SSTs onto the iAMV index. The rationale behind this approach is that variations in G are mainly a reflection of external radiative forcing, making it a convenient metric for tracking the temporal evolution of forced climate change. The extent to which internal variations in G (henceforth, iG) affect the efficacy of the G-Res method has not been elucidated, apart from Q20 who noted its impact on the inferred iAMV timeseries in observations. The purpose of this study is to explicitly clarify the impact of iG on the spatial pattern of simulated and observed iAMV, using LEs from multiple global coupled climate models as a methodological testbed.

2. Data and Methods

2.1. Model LEs and Observational Data

We analyze seven global coupled model LEs with ensemble sizes ranging from 30 to 100 and spanning the years 1950–2100 under historical and future radiative forcing (see Table S1 in Supporting Information S1 for model and forcing details). We also make use of gridded observational products of SST, sea level pressure (PSL), and terrestrial precipitation (PR) spanning 1950–2020 (Table S2 in Supporting Information S1). We compute monthly anomalies by subtracting the long-term (1950–2020 or 2030–2100) mean for each month separately, form annual averages from the monthly anomalies, and apply a 10-year low-pass Butterworth filter. All data sets are bi-linearly interpolated to the nominal 1° spatial resolution of Community Earth System Model version 2.

2.2. Methods

The true internal component (i) of low-pass filtered annual SST, PSL, and PR anomalies in each ensemble member of a given model LE are defined as:

$$\mathrm{iSST}(x,t,e) = \mathrm{SST}(x,t,e) – \mathrm{SST}(x,t,em)$$

$$\mathrm{iPSL}(x,t,e) = \mathrm{PSL}(x,t,e) – \mathrm{PSL}(x,t,em)$$

$$\mathrm{iPR}(x,t,e) = \mathrm{PR}(x,t,e) – \mathrm{PR}(x,t,em)$$

where x is grid box location, t is time, e is ensemble member, and em is the ensemble-mean.

The estimated internal component of low-pass filtered annual SST, PSL, and PR anomalies based on the G-Res method are computed as:

$$\mathrm{gresSST}(x,t,e) = \mathrm{SST}(x,t,e) – G(t,e) \times \mathrm{GSSTreg}(x,e)$$

$$\mathrm{gresPSL}(x,t,e) = \mathrm{PSL}(x,t,e) – G(t,e) \times \mathrm{GPSLreg}(x,e)$$

$$\mathrm{gresPR}(x,t,e) = \mathrm{PR}(x,t,e) – G(t,e) \times \mathrm{GPRreg}(x,e)$$

where $G(t,e)$ is the global-mean (60°N-60°S) SST, GSSTreg(x,e) is the linear regression of SST(x,t,e) onto G(t,e), GPSLreg(x,e) is the linear regression of PSL(x,t,e) onto $G(t,e)$, and GPRreg(x,e) is the linear regression of PR(x,t,e) onto $G(t,e)$.

We next construct iAMV indices for each ensemble member of a given model LE by computing NA area-weighted averages of iSST(x,t,e) and gresSST(x,t,e), hereafter referred to as iNA(t,e) and gresNA(t,e), respectively. To compute the spatial patterns of iAMV in each ensemble member of a given model LE, we linearly regress iSST(x,t,e), iPSL(x,t,e), and iPR(x,t,e) onto the standardized iNA(t,e); similarly, we regress gresSST(x,t,e), gresPSL(x,t,e), and gresPR(x,t,e) onto the standardized gresNA(t,e). These sets of regression maps will be referred to as iAMVtruth$_{NA}$ and iAMVgres, respectively. To enhance the robustness of the patterns, we then average the regression maps across the individual members of a given model LE, denoted [iAMVtruth$_{NA}$] and [iAMVgres]. We also compute the multi-model LE (MMLE) average of the seven [iAMVtruth$_{NA}$] and [iAMVgres] regression maps.

By construction, gresSST(x,t,e), gresPSL(x,t,e), and gresPR(x,t,e) contain no global-mean component. Thus, in order to provide an "apples-to-apples" comparison of the G-Res and Truth methods, we define

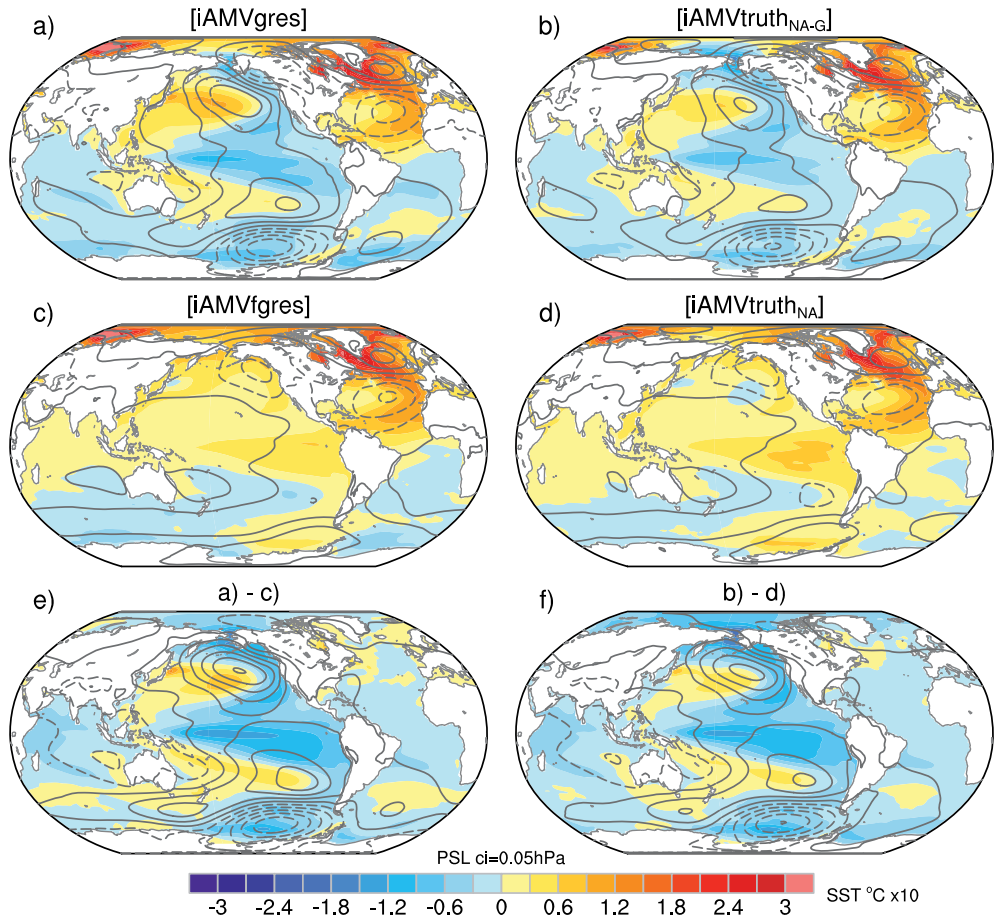

Figure 1. Multi-model Large Ensemble internal Atlantic Multidecadal Variability (iAMV) regression maps for sea surface temperature (SST) (color shading) and sea level pressure (PSL) (contours; negative values dashed) based on 1950–2020 using the following methods: (a) [iAMVgres]; (b) [iAMVtruth$_{NA-G}$]; (c) [iAMVfgres]; (d) [iAMVtruth$_{NA}$]; (e) a–c; (f) b–d. See text for explanation.

iSST*(x,t,e) = iSST(x,t,e) – iG(t,e), where iG(t,e) is the global-mean (60°N-60°S) of iSST(x,t,e) (and similarly for iPSL and iPR), as well as a new index iNA*(t,e) = iNA(t,e) – iG(t,e). We then construct regression maps of iSST*(x,t,e), iPSL*(x,t,e), and iPR*(x,t,e) onto the standardized iNA*(t,e), denoted iAMVtruth$_{NA-G}$ (and [iAMVtruth$_{NA-G}$] for the ensemble mean).

For a given model LE, G(t,e) can be decomposed into a forced component fG(t), estimated as G(t,em), and an internal component iG(t,e), estimated by subtracting G(t,em) from G(t,e). The term iG(t,e) can be further decomposed into a part that is congruent with iNA(t,e) [denoted iG$_{NA}$(t,e) and obtained by scaling iNA(t,e) by the regression of iG(t,e) onto iNA(t,e)], and a part that is orthogonal to iNA(t,e) [denoted iG*(t,e) and obtained by subtracting iG$_{NA}$(t,e) from iG(t,e)]. Unless stated otherwise, all pattern correlations (r) are based on area-weighted data over the global domain (60°N-60°S). "Interdecadal Pacific Variability" (IPV; Power et al., 1999) is defined as the leading Empirical Orthogonal Function of low-pass filtered iSST over the domain (40°S-60°N, 110°E-70°W). A glossary of acronyms is provided in Table S3 in Supporting Information S1.

3. Results

3.1. G-Res Method Versus Truth

Figure 1a shows the MMLE [iAMVgres] regression maps for SST and PSL over the period 1950–2020. The large number of simulations across the seven model LEs (420 in total) used to construct these fields ensures their robustness to sampling and model uncertainty (note that there is also good structural agreement amongst

the individual model LE [iAMVgres] regression maps; Figure S1 in Supporting Information S1). The MMLE [iAMVgres] patterns exhibit canonical signatures of AMV in the Atlantic sector, with horseshoe-shaped warming north of the equator and weaker cooling to the south, accompanied by a dipole structure in PSL over the North Atlantic that resembles the negative phase of the North Atlantic Oscillation (NAO; Figure 1a). They also show prominent expression in the Pacific reminiscent of the negative phase of IPV, with negative SST anomalies in the tropics and extending poleward along the eastern sides of the basin, accompanied by anticyclonic PSL anomalies in midlatitudes and cyclonic anomalies farther poleward in both hemispheres.

The MMLE [iAMVgres] regression patterns are very similar to those based on MMLE [iAMVtruth$_{NA\text{-}G}$] ($r = 0.96$ for SST and 0.98 for PSL), with some small (~25%) differences in amplitude over the Pacific sector (Figure 1b). This close resemblance attests to the high skill of the G-Res method in isolating the true structure of iAMV in the MMLE; high skill (r generally >0.9) is also found for each model LE individually (compare Figures S1 and S2 in Supporting Information S1, and see Table S4a in Supporting Information S1).

The MMLE [iAMVtruth$_{NA}$] regression patterns display striking differences from [iAMVtruth$_{NA\text{-}G}$] outside of the Atlantic sector, with anomalies generally of opposite sign and weaker magnitude (Figure 1d). In particular, the former shows positive and eastward-intensified SST anomalies in the tropical Pacific accompanied by negative (positive) PSL anomalies in the Gulf of Alaska (Amundsen-Bellinghausen Seas), whereas the latter shows negative and westward-amplified tropical Pacific SST anomalies, accompanied by regional PSL features that are opposite in sign and displaced equatorward and westward. Qualitatively similar contrasts between [iAMVtruth$_{NA}$] and [iAMVtruth$_{NA\text{-}G}$] are found for each model LE individually (Figure S2 in Supporting Information S1). We emphasize that there is no a priori physical justification for using iAMVtruth$_{NA\text{-}G}$ to define iAMV; our purpose here is to simply provide an "apples-to-apples" comparison with [iAMVgres], which implicitly removes variability associated with $G(t,e)$.

The stark differences between the MMLE [iAMVtruth$_{NA}$] and [iAMVtruth$_{NA\text{-}G}$] regression patterns indicate that iSST associations with iG(t,e) dominate over those with iNA(t,e) in regions outside the Atlantic (and vice versa within the Atlantic). To explicitly highlight the influence of iG(t,e), we plot the difference between MMLE [iAMVtruth$_{NA}$] and MMLE [iAMVtruth$_{NA\text{-}G}$] (Figure 1f). This difference map is dominated by a negative IPV-like structure, evidenced by the high pattern correlations with the MMLE [IPV] ($r = 0.94$ for SST and 0.98 for PSL). That the difference map resembles IPV is not surprising, given the extensive literature documenting its association with internal variations in observed and simulated G (e.g., Dai et al., 2015; Kosaka & Xie, 2013). The salient point here is that the G-Res method implicitly removes variability associated with IPV (via iG), thereby imparting a spurious negative IPV-like structure to iAMV. This distortion of iAMV by IPV in the G-Res method is also found for each model LE individually (Figure S2 in Supporting Information S1).

As discussed in Section 2.2, iG(t,e) is the sum of iG$_{NA}$(t,e) and iG*(t,e). Thus, the difference map in Figure 1f reflects not only the association of iSST(x,t,e) with iG*(t,e), but also its association with iG$_{NA}$(t,e). However, because the standard deviation (σ) of iG$_{NA}$ is small (<10%) compared to that of iG* (both for the MMLE and for each individual model LE), the difference map is dominated by variability associated with iG*(t,e).

Here, we propose a reformulation of the G-Res method such that only fluctuations associated with the forced component of G(t,e) are removed, thereby circumventing the issues discussed above. This "forced-G" Residual Method (hereafter, "fG-Res method") is defined as follows:

$$\mathrm{fgresSST}(x,t,e) = \mathrm{SST}(x,t,e) - \mathrm{fG}(t) \times \mathrm{fGreg}(x,e)$$

where fGreg(x,e) is the linear regression of SST(x,t,e) onto fG(t) for a given model LE; similar equations were obtained for PSL and PR. We then define fgresNA(t,e) as the NA area-average of fgresSST(x,t,e), and construct iAMV maps for each ensemble member by regressing fgresSST(x,t,e) (and the analogous PSL and PR fields) onto the standardized fgresNA(t,e) index. These regression maps are referred to as iAMVfgres.

The MMLE [iAMVfgres] and [iAMVtruth$_{NA}$] regression patterns are nearly identical ($r = 0.98$ for SST and 0.97 for PSL), demonstrating the high skill of the fG-Res method (compare Figures 1c and 1d); similar skill is found for each individual model LE (Table S4b; Figures S1 and S2 in Supporting Information S1). Differencing MMLE [iAMVfgres] from MMLE [iAMVgres] reveals the impact of iG on the pattern of iAMV estimated with the G-Res method. This difference map (Figure 1e) is nearly identical to that between [iAMVtruth$_{NA}$] and [iAMVtruth$_{NA\text{-}G}$], with $r = 0.97$ for SST and 0.99 for PSL; similar results are found for each model LE (Table S4c; Figures S1 and S2 in Supporting Information S1).

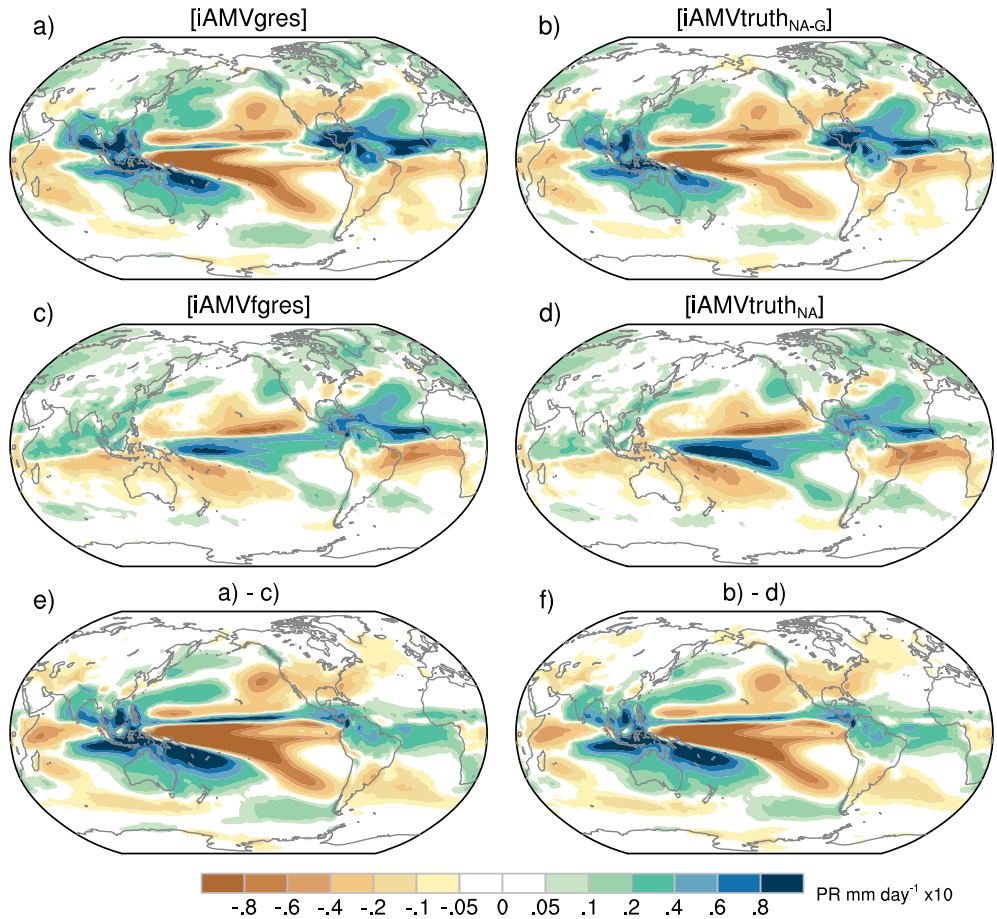

Figure 2. As in Figure 1 but for precipitation.

Results for PR are analogous to those for SST and PSL (Figure 2). In particular, the G-Res method (Figure 2a) introduces a pronounced but spurious negative IPV structure (Figure 2e) that overwhelms the true linkage to a weak positive IPV seen with the fG-Res approach (Figure 2c); it also introduces spurious drying over much of the United States (compare Figures 2a and 2c). Both G-Res and fG-Res show high skill ($r = 0.97$ and 0.96, respectively) in reproducing the MMLE iAMV PR regression patterns of their "Truth" counterparts (compare left and right columns of Figure 2); similar skill is found for each model LE individually (Figures S3 and S4; Table S4 in Supporting Information S1).

All of the above conclusions hold for the future (2030–2100) patterns of iAMV (Figures S5 and S6; Table S4 in Supporting Information S1). We also note that the iAMV SST patterns in the models' preindustrial control simulations are very similar to those in the historical (1950–2020) LEs based on the Truth method, confirming the efficacy of the Truth method for isolating internal variability (Figure S7 in Supporting Information S1).

3.2. Sampling Variability of Model iAMV Patterns

Here we address the issue of sampling variability of the iAMV SST regression maps estimated with the G-Res and fG-Res methods in each model LE by computing pattern correlations between each ensemble member (e.g., iAMVgres) and the ensemble-mean (e.g., [iAMVgres]). This metric quantifies how well the ensemble-mean iAMV SST pattern obtained with either G-Res or fG-Res can be isolated in any individual realization, given "noise" from unrelated patterns of internal variability. The distribution of pattern correlations will be particularly relevant for contextualizing the observational results in Section 3c.

Figure 3 shows the distribution of SST pattern correlations (r) for each model LE based on: (a) G-Res; (b) fG-Res; and (c) the difference between G-Res and fG-Res. Most models show a large range of r for each method, often

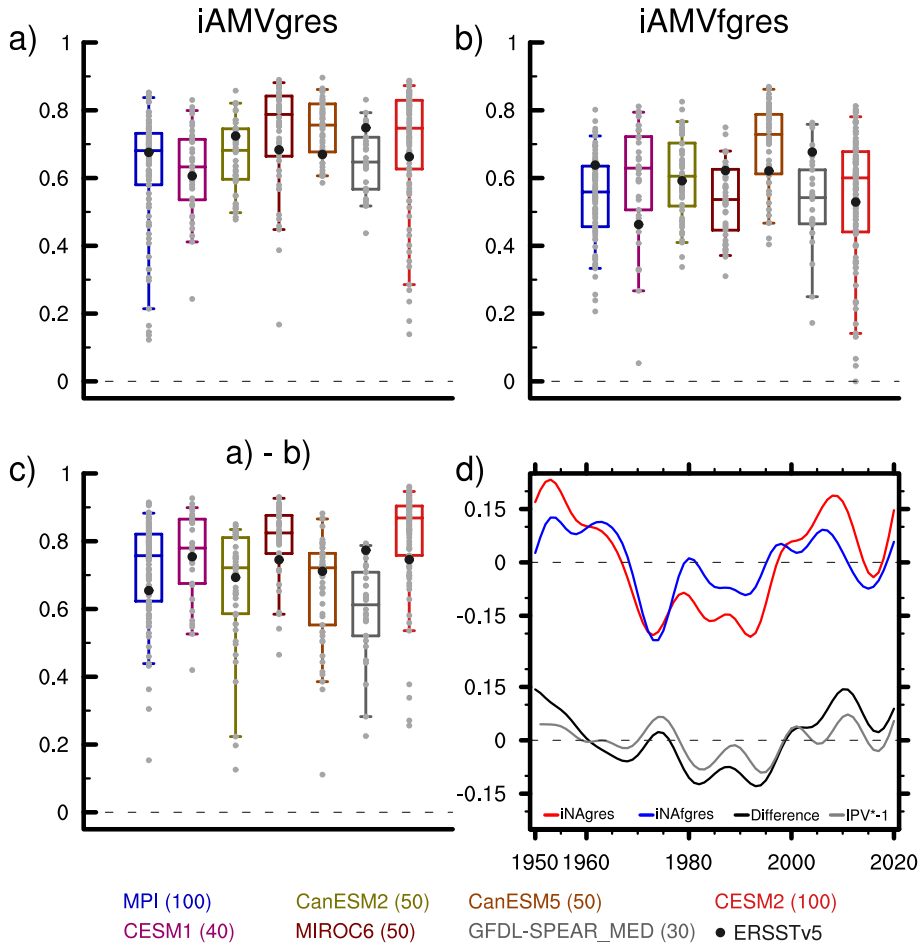

Figure 3. Distribution of internal Atlantic Multidecadal Variability (iAMV) sea surface temperature (SST) pattern correlations between each ensemble member and the ensemble-mean (gray dots) for each model Large Ensemble (LE) based on 1950–2020 using the following methods: (a) iAMVgres; (b) iAMVfgres; and (c) iAMVgres minus iAMVfgres. Boxes outline the 25th-to-75th percentile range, and whiskers show the 5th-to-95th percentile range. Black dots indicate correlations between observations and the model ensemble-means. Panel (d): (upper curves) observed iNA SST index (°C) based on iAMVgres (red) and iAMVfgres (blue); (lower curves) their difference (black) and the inverted IPV index shifted by 1 year (gray; Henley et al., 2015).

spanning values as low as 0.1 to as high as 0.9 across the individual members. For the majority of models, the 5th-to-95th percentile range of r values (which takes into account the different ensemble sizes of the various model LEs) is about 0.3–0.8, and the median value is about 0.6–0.8. These results indicate that the spatial pattern of iAMV estimated in any single model simulation may be obscured by additional sources of internal variability that are independent of iAMV. For most models, the range of r is smaller and the median r is higher for the Atlantic sector (80°W-30°E) compared to the Indo-Pacific (defined as the region outside the Atlantic; Figure S8 in Supporting Information S1).

3.3. Application of the G-Res and fG-Res Methods to Observations

We now apply the G-Res and fG-Res methods to the observations for the period 1950–2020 as follows:

$$\text{gresSST\_Obs}(x,t) = \text{SST\_Obs}(x,t) - \text{G\_Obs}(t) \times \text{GSSTreg\_Obs}(x)$$

where SST_Obs(x,t) is the observed low-pass filtered annual SST, G_Obs(t) is the global-mean (60°N-60°S) of SST_Obs(x,t), and GSSTreg_Obs(x) is the linear regression of SST_Obs(x,t) onto G_Obs(t).

$$\text{fgresSST\_Obs}(x,t) = \text{SST\_Obs}(x,t) - \text{fG}(t) \times \text{fGSSTreg\_Obs}(x)$$

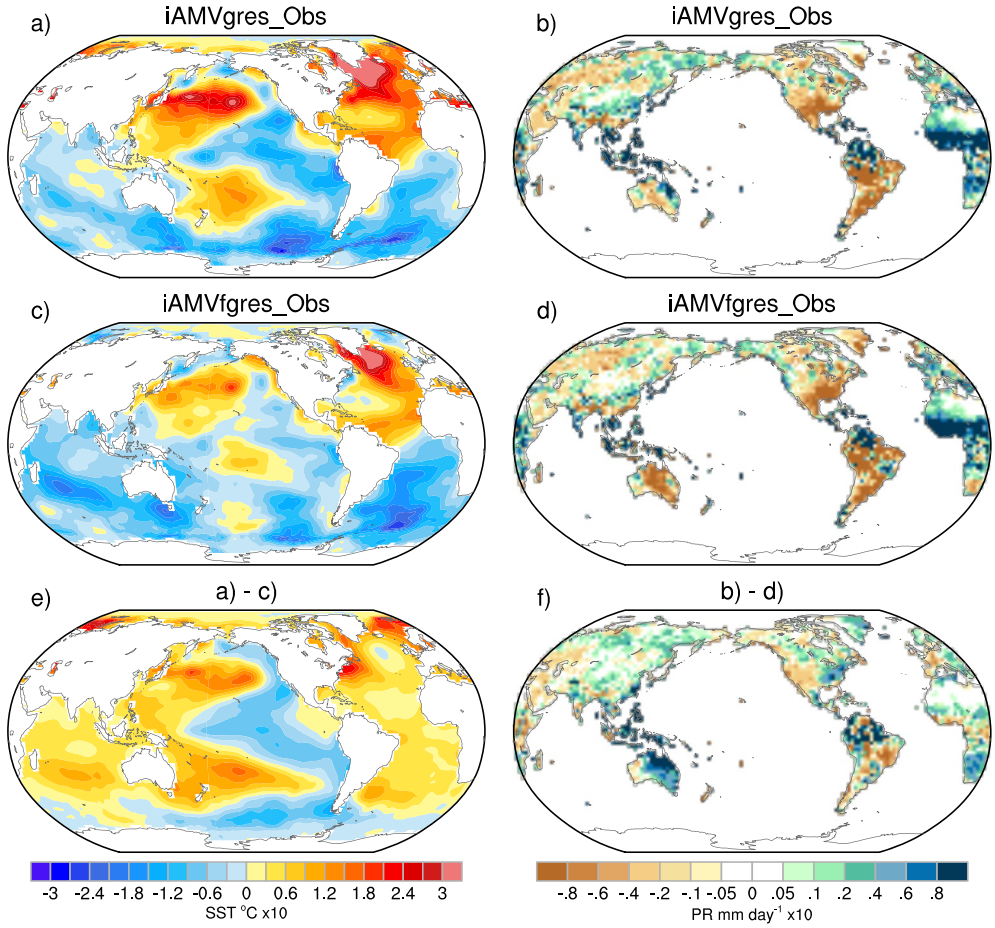

Figure 4. Observed internal Atlantic Multidecadal Variability (iAMV) sea surface temperature (SST) (left) and terrestrial precipitation (PR) (right) regression maps based on 1950–2020 using the following methods: (a and b) iAMVgres_Obs; (c and d) iAMVfgres_Obs; and (e and f) iAMVgres_Obs minus iAMVfgres_Obs. See text for explanation.

where fG(t) is the MMLE G(t,em) and fGSSTreg_Obs(x) is the linear regression of SST_Obs(x,t) onto fG(t).

We construct observed iAMV patterns by regressing gresSST_Obs(x,t) onto the normalized NA average of gresSST_Obs(x,t), and regressing fgresSST_Obs(x,t) onto the normalized NA average of fgresSST_Obs(x,t); these regression patterns are denoted iAMVgres_Obs and iAMVfgres_Obs, respectively. Analogous procedures are used for PSL and PR. Note that no model information is used to construct iAMVgres_Obs, and the only model information used to construct iAMVfgres_Obs is MMLE G(t,em). For reference, the G_Obs(t) and fG(t) timeseries are shown in Figure S9 in Supporting Information S1.

The observed iNA SST timeseries obtained with the G-Res method has a visibly larger amplitude than that obtained with the fG-Res method (standard deviation σ = 1.4°C vs. 0.9°C), and exhibits notable differences in timing including a more pronounced negative phase from the mid-1970s to the mid-1990s (compare red and blue curves in Figure 3d). The difference between the two iNA timeseries (black curve) closely resembles the observed (inverted) IPV timeseries (gray curve), with a correlation coefficient of 0.83 at zero-lag and 0.88 when the IPV Index leads by 1 year (correlation distributions in the model LEs are shown in Figure S10 in Supporting Information S1).

The iAMVgres_Obs SST pattern exhibits an interhemispheric dipole structure in the Atlantic sector and a negative IPV-like pattern in the Indo-Pacific accompanied by negative anomalies across the Southern Ocean (Figure 4a). Compared to iAMVgres_Obs, iAMVfgres_Obs shows a weaker and more amorphous structure in the Pacific sector (Figure 4c). Their difference (iAMVgres_Obs minus iAMVfgres_Obs) displays a pronounced negative IPV pattern (also for PSL, see Figure S11 in Supporting Information S1), as well as positive SST

anomalies along the US east coast and Norwegian Sea (Figure 4c). Thus, the observational results are largely analogous to the findings based on the seven model LEs, namely that inclusion of internal G variability via the G-Res method imparts a spurious negative IPV-like connection to iAMV. The observational results bear an even stronger resemblance to the model LE results when the analysis period is extended back to 1900 (Figure S12 in Supporting Information S1).

As noted above, one should not expect a perfect match between the observational and model results, even if the model has a "perfect" representation of iAMV, due to the presence of sampling variability (recall Figure 3). Indeed, the iAMV SST pattern correlation between observations and the ensemble-mean of each LE falls within the 5th-to-95th (and mostly within the 25th-to-75th) percentile range of the distribution for each model, regardless of the method used (black circles in Figures 3a–3c); the same holds for the Atlantic and Indo-Pacific domains (Figure S8 in Supporting Information S1). This indicates that the observed iAMV SST regression patterns (including the difference between the G-Res and fG-Res methods) are consistent with those drawn from the population of individual members of each model LE.

The observed iAMV PR regression maps also show notable differences between the G-Res and fG-Res methods (Figures 4b and 4d). In particular, the inclusion of "observed" internal G in the definition of iAMV introduces spurious drying over the western US, enhanced wetting over the Amazon and eastern Australia, and a tripolar pattern over the African continent (wetting over the Sahel, drying over equatorial Africa and wetting over South Africa), all consistent with a negative IPV and similar to the model LE results (Figure 4f).

4. Summary and Discussion

We have shown that the G-Res method, widely used for isolating internal modes of climate variability, distorts the spatial pattern of iAMV (conventionally defined based on low-pass filtered NA SST) by introducing spurious signals over the Indo-Pacific basin in seven different model LEs and in observations. This distortion occurs because the global-mean SST timeseries used in the method to define (and remove) the spatial pattern of externally-forced climate variability contains internal variability in addition to a forced response. The internal component of $G(t)$ is predominantly associated with fluctuations in the leading mode of Indo-Pacific SST variability (IPV), consistent with previous literature. This deficiency of the G-Res method can be overcome by using the forced component of $G(t)$ in place of the total $G(t)$. This modified version of the G-Res method (termed fG-Res) skillfully reveals the true spatial pattern of iAMV in each of the seven model LEs, a pattern which is primarily confined to the NA and adjacent Arctic Ocean. Some models also show a weak connection to the tropical Pacific and the far northern Pacific. Importantly, these Pacific connections are opposite in sign to those obtained with the conventional G-Res method.

All seven model LEs show high member-to-member variability in their simulated iAMV SST regression patterns based on 1950–2020 (and 2030–2100; not shown), indicating that a single 70-year realization is not adequate to isolate iAMV from other sources of internal variability. Because the observational record captures only one of many possible trajectories of internal variability during 1950–2020 (superimposed upon an externally-forced response), assessment of model fidelity must take into account sampling uncertainty. By this measure, all of the models examined produce realistic iAMV SST patterns according to the fG-Res method. Further, they also simulate realistic amplitudes of iNA SST variability based on the fG-Res method, evidenced by the fact that the observed iNA σ lies within the 5th-to-95th percentile range of iNA σ values across the individual members of each model LE (not shown).

What is the minimum ensemble size needed to robustly estimate [iAMVfgres] and iAMVfgres_Obs? Using random sampling procedures described in the Supporting Information S1, we find that approximately 20 members are needed to reproduce the SST pattern of [iAMVfgres] in each model LE (Figure S13 in Supporting Information S1), and that six members are needed to compute fG(t) in the calculation of the SST iAMVfgres_Obs pattern (Figure S14 in Supporting Information S1; note that this pattern is still subject to the same level of sampling variability as that shown in Figure 3b).

It is beyond the scope of this study to undertake a detailed investigation of the underlying physical causes of iAMV in the model LEs. Here, we briefly examine the role of the Atlantic Meridional Overturning Circulation (AMOC) since it has been identified as a key mechanism for iAMV-related SST fluctuations in the NA (especially, the subpolar NA; SPNA) via changes in ocean heat transport that may be predictable out to decadal lead

times (e.g., Kim et al., 2020; Yeager et al., 2020). Using the our "Truth" methodology, we have constructed MMLE regression maps of SST and PSL upon the models' standardized iAMOC timeseries leading by 4 years (the lag of maximum correlation between iNA SST and iAMOC; not shown). These iAMOC regression patterns show the expected SST warming over the NA (especially the SPNA) and adjacent Arctic Ocean, with a weak positive PSL anomaly over the midlatitude NA (Figure S15b in Supporting Information S1); however, the magnitude of the AMOC-related warming is <50% of the warming associated with a 1σ departure of the iNA SST index (Figure S15a in Supporting Information S1). Differencing the NA and AMOC regression maps reveals a tripolar SST pattern over the NA accompanied by a negative NAO-like PSL pattern (Figure S15c in Supporting Information S1), qualitatively consistent with the thermodynamic response of the upper-ocean mixed layer to atmospheric forcing (e.g., Clement et al., 2015; Deser et al., 2010). This difference map also shows a weak positive ENSO-like signature in the Indo-Pacific (SST warming in the tropical eastern Pacific, weakened tropical Pacific PSL gradient, and negative PSL anomalies in the eastern North Pacific), which may reflect the well-known teleconnection from the Pacific to the Atlantic (e.g., Deser et al., 2010; Meehl et al., 2021). In support of this causal inference, we note that the "Truth method" regression map of net surface heat flux upon the iNA SST index exhibits positive (downward) values over the tropical North Atlantic, implying that the atmosphere is driving the iAMV SSTs in this region and not vice versa (not shown). This direction of causality is consistent with IPV "Pacemaker" (but inconsistent with AMV "Pacemaker") experiments reported in Meehl et al. (2021). Thus, caution is needed when interpreting the relevance of regional "Pacemaker" experiments. In summary, our results support the notion that both AMOC and thermodynamic air-sea interaction independent of AMOC contribute to the simulated pattern of iAMV defined on the basis of iNA SST. Application of the fG-Res method to define iAMV in paleoclimate simulations (Fang et al., 2021; Wang et al., 2017) is left to future work.

Data Availability Statement

All observational data sets used in this study are publicly available from: www.ncei.noaa.gov/products/extended-reconstructed-sst; www.dwd.de/EN/ourservices/gpcc/gpcc.html; and www.ecmwf.int/en/forecasts/dataset/ecmwf-reanalysis-v5. All model simulations used in this study are publicly available from: https://www.cesm.ucar.edu/community-projects/mmlea; and https://esgf-node.llnl.gov/search/cmip6/. Analysis code is posted at https://www.cesm.ucar.edu/projects/cvdp-le/code.

Acknowledgments
We thank the anonymous reviewers for their constructive comments and suggestions. The National Center for Atmospheric Research is sponsored by the National Science Foundation.

References

Baek, S. H., Kushnir, Y., Ting, M., Smerdon, J. E., & Lora, J. M. (2022). Regional signatures of forced North Atlantic SST variability: A limited role for aerosols and greenhouse gases. *Geophysical Research Letters*, *49*(8), e2022GL097794. https://doi.org/10.1029/2022GL097794

Clement, A., Bellomo, K., Murphy, L. N., Cane, M. A., Mauritsen, T., Radel, G., & Stevens, B. (2015). The Atlantic multidecadal oscillation without a role for ocean circulation. *Science*, *350*(6258), 320–324. https://doi.org/10.1126/science.aab3980

Dai, A., Fyfe, J. C., Xie, S.-P., & Dai, X. (2015). Decadal modulation of global surface temperature by internal climate variability. *Nature Climate Change*, *5*(6), 555–559. https://doi.org/10.1038/nclimate2605

Deser, C., Alexander, M. A., Xie, S.-P., & Phillips, A. S. (2010). Sea surface temperature variability: Patterns and mechanisms. *Annual Review of Marine Science*, *2*(1), 115–143. https://doi.org/10.1146/annurev-marine-120408-151453

Deser, C., Lehner, F., Rodgers, K. B., Ault, T., Delworth, T. L., DiNezio, P. N., et al. (2020). Insights from Earth system model initial-condition large ensembles and future prospects. *Nature Climate Change*, *10*(4), 277–286. https://doi.org/10.1038/s41558-020-0731-2

Deser, C., & Phillips, A. S. (2021). Defining the internal component of Atlantic Multidecadal Variability in a changing climate. *Geophysical Research Letters*, *48*(22), e2021GL095023. https://doi.org/10.1029/2021GL095023

Enfield, D. B., Mestas-Nuñez, A. M., & Trimble, P. J. (2001). The Atlantic multidecadal oscillation and its relation to rainfall and river flows in the continental US. *Geophysical Research Letters*, *28*(10), 2077–2080. https://doi.org/10.1029/2000GL012745

Fang, S. W., Khodri, M., Timmreck, C., Zanchettin, D., & Jungclaus, J. (2021). Disentangling internal and external contributions to Atlantic multidecadal variability over the past millennium. *Geophysical Research Letters*, *48*(23), e2021GL095990. https://doi.org/10.1029/2021gl095990

Frankignoul, C., Gastineau, G., & Kwon, Y. O. (2017). Estimation of the SST response to anthropogenic and external forcing and its impact on the Atlantic multidecadal oscillation and the Pacific decadal oscillation. *Journal of Climate*, *30*(24), 9871–9895. https://doi.org/10.1175/jcli-d-17-0009.1

Henley, B. J., Gergis, J., Karoly, D. J., Power, S., Kennedy, J., & Folland, C. K. (2015). A tripole index for the interdecadal Pacific oscillation. *Climate Dynamics*, *45*(11–12), 3077–3090. https://doi.org/10.1007/s00382-015-2525-1

Kim, W. M., Yeager, S., & Danabasoglu, G. (2020). Atlantic Multidecadal Variability and associated climate impacts initiated by ocean thermohaline dynamics. *Journal of Climate*, *33*(4), 1317–1334. https://doi.org/10.1175/jcli-d-19-0530.1

Kosaka, Y., & Xie, S.-P. (2013). Recent global-warming hiatus tied to equatorial Pacific surface cooling. *Nature*, *501*(7467), 403–407. https://doi.org/10.1038/nature12534

Meehl, G., Hu, A., Castruccio, F., England, M., Bates, S., Danabasoglu, G., et al. (2021). Atlantic and Pacific tropics connected by mutually interactive decadal-timescale processes. *Nature Geoscience*, *14*(1), 36–42. https://doi.org/10.1038/s41561-020-00669-x

Murphy, L. N., Bellomo, K., Cane, M., & Clement, A. (2017). The role of historical forcings in simulating the observed Atlantic multidecadal oscillation. *Geophysical Research Letters*, *44*, 2472–2480. https://doi.org/10.1002/2016GL071337

Power, S., Casey, T., Folland, C., Colman, A., & Mehta, V. (1999). Inter-decadal modulation of the impact of ENSO on Australia. *Climate Dynamics*, *15*(5), 319–324. https://doi.org/10.1007/s003820050284

Qin, M., Dai, A., & Hua, W. (2020). Quantifying contributions of internal variability and external forcing to Atlantic Multidecadal Variability since 1870. *Geophysical Research Letters*, *47*(22), e2020GL089504. https://doi.org/10.1029/2020GL089504

Trenberth, K. E., & Shea, D. J. (2006). Atlantic hurricanes and natural variability in 2005. *Geophysical Research Letters*, *33*(12), L12704. https://doi.org/10.1029/2006GL026894

Yan, X., Zhang, R., & Knutson, T. R. (2019). A multivariate AMV index and associated discrepancies between observed and CMIP5 externally forced AMV. *Geophysical Research Letters*, *46*, 4421–4431. https://doi.org/10.1029/2019GL082787

Wang, J., Yang, B., Ljungqvist, F. C., Luterbacher, J., Osborn, T. J., Briffa, K. R., & Zorita, E. (2017). Internal and external forcing of multidecadal Atlantic climate variability over the past 1,200 years. *Nature Geoscience*, *10*(7), 512–517. https://doi.org/10.1038/ngeo2962

Yeager, S. (2020). The abyssal origins of North Atlantic decadal predictability. *Climate Dynamics*, *55*(7–8), 2253–2271. https://doi.org/10.1007/s00382-020-05382-4

Zhang, R., Sutton, R., Danabasoglu, G., Kwon, Y.-O., Marsh, R., Yeager, S. G., et al. (2019). A review of the role of the Atlantic Meridional Overturning Circulation in Atlantic multidecadal variability and associated climate impacts. *Reviews of Geophysics*, *57*(2), 316–375. https://doi.org/10.1029/2019RG000644